

SYMMETRIC GALERKIN BOUNDARY INTEGRAL FORMULATION FOR INTERFACE AND MULTI-ZONE PROBLEMS

L. J. Gray* Glaucio H. Paulino[†]

April 6, 1999

Abstract

Domains containing an ‘internal boundary’, such as a bi-material interface, arise in many applications, *e.g.* composite materials and geophysical simulations. This paper presents a symmetric Galerkin boundary integral method for this important class of problems. In this situation, the physical quantities are known to satisfy continuity conditions across the interface, but no boundary conditions are specified. The algorithm described herein achieves a symmetric matrix of reduced size. Moreover, the symmetry can also be invoked to lessen the numerical work involved in constructing the system of equations, and thus the method is computationally very efficient. A prototype numerical example, with several variations in the boundary conditions and material properties, is employed to validate the formulation and corresponding numerical procedure. The boundary element results are compared with analytical solutions and with numerical results obtained with the finite element method.

Key words. Boundary integral method, symmetric-Galerkin approximation, interfaces, multi-zone boundary element analysis, composite materials.

*Computer Science and Mathematics Division, Oak Ridge National Laboratory, Oak Ridge, Tennessee 37831-6367, U.S.A.

[†]Department of Civil and Environmental Engineering, University of California, Davis, CA 95616-5294, U.S.A.

in the formulation, and thus the interface conditions can be incorporated simply and accurately. This issue is quite important in practical applications. For instance, for a bi-material interface crack problem, the interface lies in the critical region ahead of the crack tip where an accurate solution is imperative.

For the boundary integral method, there is another important class of problems for which an efficient interface algorithm is required, namely for long thin domains [2]. These problems can be solved by means of a *multi-zone* boundary element analysis. Although adding surface area is generally a bad idea, in this situation it is computationally efficient to decompose the domain into small subdomains by means of artificial interfaces (Figure 2). The reason is that constructing the boundary integral equations for each subdomain only requires integrating over a small piece of the boundary, and this more than compensates for the presence of the additional boundary surface. Note too that the resulting coefficient matrix has a block-sparse structure, adding to the computational efficiency.

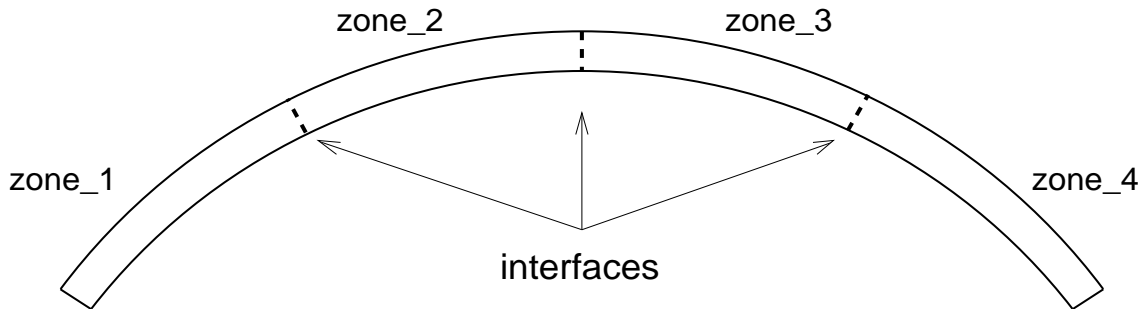


Figure 2: Division of a thin geometry into zones for multi-zone boundary element analysis.

The symmetric Galerkin (SG) method is a highly robust and efficient boundary integral approximation. It was introduced by Hartmann *et al.* in 1985 [3], and further developed by Maier and co-workers [4] and many others. A key advantage of the Galerkin formulation is the ability to treat hypersingular equations with standard *continuous* elements (*e.g.* linear, quadratic). The more commonly used collocation approximation [5] requires a *differentiable* boundary interpolation [6, 7], which is inherently difficult and computationally expensive (*e.g.* Hermite [8, 9] or Overhauser [10, 11] elements). Considering the essential role of hypersingular equations in the efficient solution of fracture and other problems [12, 6, 13], this is a significant advantage of Galerkin type formulations. Compared to collocation methods with standard continuous elements, Galerkin is also quite expensive, but the added symmetric aspect makes this approach computationally efficient. Although non-symmetric Galerkin is roughly an order of magnitude slower than collocation, SG is as fast or faster [14, 15]. As a consequence, SG is an ideal algorithm for crack geometries

[16, 17]. In addition, the FEM will produce a symmetric coefficient matrix, and thus SG is especially advantageous for coupling boundary integral analysis with finite elements [18].

As will be explained in more detail below, for standard boundary value problems, a symmetric matrix is obtained by suitably combining the standard boundary integral equation (BIE) and its derivative, the hypersingular boundary integral equation (HBIE). The choice of equation enforced at a node depends upon the boundary condition at this point. For the Dirichlet-type surface (*i.e.* specified potential, displacement, etc.) the BIE is employed, whereas the HBIE is written on the Neumann-type surface (*i.e.* specified flux, traction, etc.).

For the general class of interface problems, however, *no data* is supplied on the ‘internal boundaries’ (see Figures 1 and 2). A natural question therefore arises – *is it possible to develop a fully symmetric Galerkin formulation for interface problems?* This paper will demonstrate that the SG approach does have a natural extension to interface geometries. Moreover, this formulation is computationally very efficient: the coefficient matrix is of reduced size, solving for values only on one side of the interface, and the symmetry can be invoked to lessen the computational work required to set up the equations.

2 Symmetric Galerkin

The boundary integral equations in this work are considered in a *limit to the boundary* sense [19, 20]. This approach allows a unified and direct treatment of the singular integrals which appear in both the BIE and the HBIE. Moreover, this technique permits writing the same equation for points either inside the domain *or* on the boundary, bypassing potential difficulties with the geometry dependent coefficient of the ‘free term’ outside the integral [20, 21]. The discussion below will consider the Laplace equation for the potential ϕ , $\nabla^2\phi = 0$, but it will be clear that the method is generally valid. This choice is not only for simplicity of notation, but also because an issue (to be discussed below) involving the material parameters arises in the potential formulation that does not appear in elasticity. This will require a slight reformulation of the BIEs for potential problems. The singular BIE can be written in the form [5]

$$\phi(P) + \int_{\Gamma} \phi(Q) \frac{\partial G}{\partial \mathbf{n}}(P, Q) dQ = \int_{\Gamma} G(P, Q) \frac{\partial \phi}{\partial \mathbf{n}}(Q) dQ , \quad (1)$$

where $\mathbf{n} = \mathbf{n}(Q)$ is the unit normal at a point Q on the domain boundary Γ , and $\partial(\cdot)/\partial \mathbf{n}$ denotes the normal derivative with respect to Q . The fundamental solution $G(P, Q)$ depends upon the dimension of the problem, and is not unique. For the following discussion, we need to remark that this function, and its derivatives, satisfy certain symmetry

properties, *i.e.*

$$\begin{aligned}
G(P, Q) &= G(Q, P) \\
\partial G(P, Q)/\partial \mathbf{n} &= -\partial G(Q, P)/\partial \mathbf{n} \\
\partial^2 G(P, Q)/\partial \mathbf{N} \partial \mathbf{n} &= \partial^2 G(Q, P)/\partial \mathbf{N} \partial \mathbf{n} \\
\partial G(P, Q)/\partial \mathbf{N} &= -\partial G(Q, P)/\partial \mathbf{N} \\
\partial G(P, Q)/\partial \mathbf{N} &= -\partial G(P, Q)/\partial \mathbf{n} \quad ,
\end{aligned} \tag{2}$$

where $\partial(\cdot)/\partial \mathbf{N}$ indicates the normal derivative with respect to P .

The corresponding hypersingular equation is obtained by differentiating Eq. (1) with respect to P in the direction $\mathbf{N} = \mathbf{n}(P)$, the normal to the boundary at P . This results in

$$\frac{\partial \phi}{\partial \mathbf{N}}(P) + \int_{\Gamma} \phi(Q) \frac{\partial^2 G}{\partial \mathbf{N} \partial \mathbf{n}}(P, Q) dQ = \int_{\Gamma} \frac{\partial G}{\partial \mathbf{N}}(P, Q) \frac{\partial \phi}{\partial \mathbf{n}}(Q) dQ . \tag{3}$$

The above HBIE is an equation for the normal derivative, but it is the flux

$$\mathcal{F}(P) \equiv \kappa \frac{\partial \phi}{\partial \mathbf{N}}(P) \tag{4}$$

which satisfies the continuity conditions across a bi-material interface. The constant κ , which goes by various names (*e.g.*, thermal conductivity) depending upon the application (*e.g.* heat transfer, electrostatics, potential flow), is different in each material. The continuity equations on the interface are then

$$\phi_A = \phi_B \tag{5}$$

and

$$\kappa_A \frac{\partial \phi_A}{\partial \mathbf{n}} = -\kappa_B \frac{\partial \phi_B}{\partial \mathbf{n}} , \tag{6}$$

where the subscripts A and B refer to the top and bottom layer in Figure 3.

By contrast, the material properties in an elasticity formulation are already embedded in the fundamental solution, and the hypersingular equation is most often written directly for the traction [12, 17]. Thus, rather than Eq. (6), the interface equation would simply be $\tau_A = -\tau_B$, where τ denotes the traction vector.

For the SG interface method, it will be convenient to rewrite the BIE, Eq. (1), and the HBIE, Eq. (3), in terms of the flux, *i.e.*

$$\phi(P) + \int_{\Gamma} \phi(Q) \frac{\partial G}{\partial \mathbf{n}}(P, Q) dQ = \int_{\Gamma} \left[\frac{1}{\kappa} G(P, Q) \right] \mathcal{F}(Q) dQ \tag{7}$$

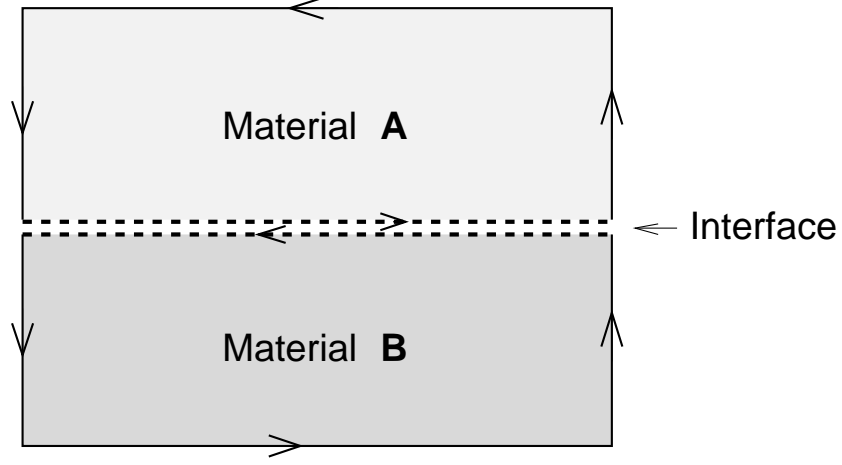


Figure 3: Bi-material interface problem.

and

$$\mathcal{F}(P) + \int_{\Gamma} \phi(Q) \left[\kappa \frac{\partial^2 G}{\partial \mathbf{N} \partial \mathbf{n}}(P, Q) \right] dQ = \int_{\Gamma} \frac{\partial G}{\partial \mathbf{N}}(P, Q) \mathcal{F}(Q) dQ , \quad (8)$$

respectively. Note that including the constant κ with G and $\partial G^2 / \partial \mathbf{N} \partial \mathbf{n}$ does not alter the basic properties required for the symmetric Galerkin method, Eqs. (2). These kernel functions are still symmetric with respect to P and Q , and the integrals containing a single derivative of G (which also play a role in achieving symmetry) remain unchanged. While this is a trivial rewriting of the boundary integral equations, it is key for directly embedding the interface continuity equations into the formulation and for obtaining a symmetric matrix.

In a Galerkin approximation, Eqs. (7) and (8) are satisfied in an averaged sense. Specifically, the weighting functions are chosen to be the basis shape functions ψ_l (*e.g.* linear, quadratic) employed in the approximation of ϕ and \mathcal{F} on the boundary. Thus,

$$\begin{aligned} \int_{\Gamma} \psi_l(P) \phi(P) dP + \int_{\Gamma} \psi_l(P) \int_{\Gamma} \phi(Q) \frac{\partial G}{\partial \mathbf{n}}(P, Q) dQ dP = \\ \int_{\Gamma} \psi_l(P) \int_{\Gamma} \left[\frac{1}{\kappa} G(P, Q) \right] \mathcal{F}(Q) dQ dP \end{aligned} \quad (9)$$

and

$$\begin{aligned} \int_{\Gamma} \psi_l(P) \mathcal{F}(P) dP + \int_{\Gamma} \psi_l(P) \int_{\Gamma} \phi(Q) \left[\kappa \frac{\partial^2 G}{\partial \mathbf{N} \partial \mathbf{n}}(P, Q) \right] dQ dP = \\ \int_{\Gamma} \psi_l(P) \int_{\Gamma} \frac{\partial G}{\partial \mathbf{N}}(P, Q) \mathcal{F}(Q) dQ dP . \end{aligned} \quad (10)$$

The additional boundary integration, with respect to P , is the last ingredient required to obtain a symmetric matrix. After discretization, the set of equations in matrix form can be written as $[H]\{\phi\} = [G]\{\mathcal{F}\}$, and in block-matrix form these equations become

$$\begin{bmatrix} H_{11} & H_{12} \\ H_{21} & H_{22} \end{bmatrix} \begin{Bmatrix} \phi_{bv} \\ \phi_u \end{Bmatrix} = \begin{bmatrix} G_{11} & G_{12} \\ G_{21} & G_{22} \end{bmatrix} \begin{Bmatrix} \mathcal{F}_u \\ \mathcal{F}_{bv} \end{Bmatrix}. \quad (11)$$

The first row represents the BIE written on the Dirichlet surface, and the second represents the HBIE on the Neumann surface. Similarly the first and second columns arise from integrating over Dirichlet and Neumann surfaces. The subscripts in the vectors therefore denote known boundary values (bv) and unknown (u) quantities. Rearranging Eq. (11) into the form $[A]\{x\} = \{b\}$, and multiplying the hypersingular equations by -1 , one obtains

$$\begin{bmatrix} -G_{11} & H_{12} \\ G_{21} & -H_{22} \end{bmatrix} \begin{Bmatrix} \mathcal{F}_u \\ \phi_u \end{Bmatrix} = \begin{Bmatrix} -H_{11} \phi_{bv} + G_{12} \mathcal{F}_{bv} \\ H_{21} \phi_{bv} - G_{22} \mathcal{F}_{bv} \end{Bmatrix}. \quad (12)$$

The symmetry of the coefficient matrix, $G_{11} = G_{11}^T$, $H_{22} = H_{22}^T$, and $H_{12} = G_{21}$, now follows from the properties of the kernel functions (Eqs. (2)).

3 Interface and Symmetry

To describe the interface algorithm, it suffices to deal with a geometry having a single common boundary, as in Figure 3. The extension to more complicated interface geometries, if not immediately obvious, is nevertheless seen to be relatively straightforward after a little thought. This topic will be further discussed in Section 4. For convenience, we will refer to the two subdomains A and B as the top and bottom regions, respectively, as shown in Figure 3. The basic idea is to write the usual SG equations on the non-interface boundaries in each subdomain, together with an appropriate combination of equations on the common boundary, as indicated by Table 1. In addition, only one set of variables is employed on the interface, *i.e.* potential and flux on the top side. Whenever the interface flux on the bottom side appears in an equation, it is replaced by the negative of the top flux.

It will again be convenient to use block-matrix notation, and only the coefficient matrix (the analogue of the left hand side in Eq. (12)) will be considered. For the interface problem, the matrix is partitioned into a 4×4 block structure and takes the form,

$$\begin{bmatrix} S_{AA} & 0 & S_{A\mathcal{F}_I} & S_{A\phi_I} \\ 0 & S_{BB} & -S_{B\mathcal{F}_I} & S_{B\phi_I} \\ \hline S_{\mathcal{F}_IA} & S_{\mathcal{F}_IB} & S_{\mathcal{F}_I\mathcal{F}_I} & S_{\mathcal{F}_I\phi_I} \\ S_{\phi_IA} & S_{\phi_IB} & S_{\phi_I\mathcal{F}_I} & S_{\phi_I\phi_I} \end{bmatrix}. \quad (13)$$

Table 1: Symmetric Galerkin integral equations for an interface or multi-zone problem.

Surface	Integral Equations
Dirichlet	BIE
Neumann	HBIE
Interface (\mathcal{F}_I) (ϕ_I)	BIE(top) – BIE(bottom) HBIE(top) + HBIE(bottom)

The first row corresponds to the SG equations written for the *non-interface* boundary in the top (A) domain, Eq. (9) or Eq. (10), depending upon the boundary conditions. The first column therefore indicates integrations involving unknown quantities on the top (non-interface) boundary. The second row and column (B) are the analogous entries for the bottom material. Thus, S_{AA} and S_{BB} are (square) symmetric matrices, a consequence of the SG procedure. The off-diagonal (1, 2) and (2, 1) blocks are, as shown, equal to zero, as the top equations do not involve the bottom geometry, and vice versa.

The third and fourth columns refer to the unknown interface flux (\mathcal{F}_I) and interface potential (ϕ_I), respectively. The top and bottom equations (*i.e.* the first and second rows) integrate over the interface and thus the (1, 3), (1, 4), (2, 3), and (2, 4), entries are in general non-zero. At the risk of being repetitive, these rows do *not* include equations for the interface, *i.e.* equations (9) and (10) with the weighting functions ψ_l centered on an interface node. The minus sign multiplying $S_{B\mathcal{F}_I}$ is due to the change in sign for the interface flux, as mentioned above. The key to achieving a symmetric matrix is to fill in rows three and four with appropriate interface equations (Galerkin weighting functions ψ_l centered on interface nodes) for determining ϕ_I and \mathcal{F}_I . The successful procedure is as follows (see Table 1).

For the interface flux, row three, write the BIE (9) for the top domain, *minus* this equation constructed for the bottom domain. This is reasonable, as equations for flux in the usual SG procedure indicate that potential is specified, and therefore the BIE is employed. Thus, it follows that $S_{\mathcal{F}_IA} = S_{A\mathcal{F}_I}^T$, the T superscript indicating transpose, as this is the SG procedure for the top domain. One can convince oneself of this simply by assuming that the top boundary is either all Dirichlet or all Neumann, and noting which integration kernel comes into play in forming this matrix. Symmetry also holds for the $S_{\mathcal{F}_IB}$ contribution, as taking the negative BIE over the bottom domain compensates for the negative sign in the (2, 3) position. It is required that the diagonal block $S_{\mathcal{F}_I\mathcal{F}_I}$ be symmetric on its own, and this easily follows from the observation that this entry comes from integrating the symmetric kernel $G(P, Q)/\kappa$ over the interface.

For the interface potential, row four, write the HBIE (10) for the top domain, *plus* this equation constructed for the bottom domain. Again, as these equations are thought of as the equations to determine the interface potential, the use of the hypersingular equation is consistent with the usual SG procedure. That $S_{\phi_I A} = S_{A\phi_I}^T$ and $S_{\phi_I B} = S_{B\phi_I}^T$ follows again from the basic SG algorithm. The symmetry of the (4, 4) block follows immediately by noting that this matrix arises from integrating the symmetric kernel $\kappa \partial^2 G(P, Q) / \partial \mathbf{N} \partial \mathbf{n}$ over the interface.

It therefore remains to show that $S_{\mathcal{F}_I \phi_I} = S_{\phi_I \mathcal{F}_I}^T$. Note first that $S_{\mathcal{F}_I \phi_I}$ originates from the left hand side of Eq. (9). However, as the single integral term is the same for both top and bottom equations, this term drops out, leaving just the $\partial G / \partial \mathbf{n}$ integration. On the other hand, $S_{\phi_I \mathcal{F}_I}$ comes from the flux terms in Eq. (10). The single integral term once again drops out, this time because of the change in sign of the flux across the interface, and thus both matrices come from the first derivative kernel. Moreover, the difference of the two equations used for the third row is once again matched by the change in sign in the flux, and so the symmetry follows.

It is interesting to note that, for the Laplace equation and a flat interface, $S_{\phi_I \mathcal{F}_I} = 0$. The normal derivative of the Green's function is given by

$$\frac{\partial G}{\partial \mathbf{n}} = -\frac{1}{2\pi} \frac{\mathbf{n} \cdot \mathbf{R}}{r^2} \quad (14)$$

where $r = \|\mathbf{R}\| = \|Q - P\|$. Due to the $\mathbf{n} \cdot \mathbf{R}$ factor, the only surviving term in integrating over a flat surface is the singular contribution. However, as in the single integral term, the singular part is the same on both sides of the interface (note that the material constant κ is not present), and therefore cancels. In some applications, this observation could be invoked to reduce the computational effort.

4 Remarks

Remark 1 Multiple Interfaces

As mentioned above, the extension of the interface algorithm to more complicated geometries is not difficult, but nevertheless warrants some further discussion. Consider the problem with three zones, labeled A , B , and C , illustrated in Figure 4. The non-interface boundary segments for each subdomain are denoted by a , b , c , respectively, and d , e , f denote the interfaces. As before, the usual SG procedure is followed on the non-interface segments, and combinations of BIE and HBIE (see Table 1) are used on the interfaces.

Thus, for example, the equations written for the interface segment d are potential and flux equations for regions A and C , while the equations for e involve regions A and B .

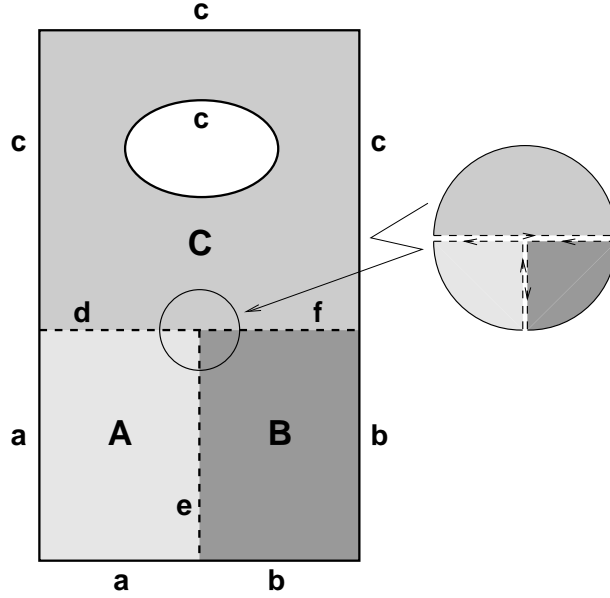


Figure 4: A more complicated interface problem.

The coefficient matrix for this problem takes the form

$$\left[\begin{array}{ccc|ccc} S_{aa} & 0 & 0 & S_{ad} & S_{ae} & 0 \\ 0 & S_{bb} & 0 & 0 & S_{be} & S_{bf} \\ 0 & 0 & S_{cc} & S_{cd} & S_{ce} & S_{cf} \\ \hline S_{da} & 0 & S_{dc} & S_{dd} & S_{de} & S_{df} \\ S_{ea} & S_{eb} & 0 & S_{ed} & S_{ee} & S_{ef} \\ 0 & S_{fb} & S_{fc} & S_{fd} & S_{fe} & S_{ff} \end{array} \right] \quad (15)$$

Here, to simplify notation, the unknown potential and flux on the interface segments have been combined. Thus, the fourth block column corresponds to potential and flux on the d interface. The symmetry of the upper-left 3×3 block again follows from the SG procedure. Verification of the symmetry for the rest of the matrix requires more thought, but follows along the same lines as the reference problem discussed in Section 3.

Remark 2 Corners

As illustrated by the above example (Figure 4), multiple interface configurations can produce difficult corner problems. For three dimensional problems, even more complicated

corner/edge configurations can occur. With respect to the A and B sub-regions of Figure 4, there are two unknown fluxes to be determined at the corner point where all three sub-domains meet. This situation is analogous to a boundary value problem in which Dirichlet data is supplied at a boundary corner. For a collocation approximation, this situation requires special treatment [22], as additional equations must be written to determine the unknown values. Another distinct advantage of the Galerkin formulation is that the extra equations are easily handled by proper definition of the Galerkin weighting functions at the corner point. All that is required is appropriate use of ‘double nodes’ in the discretization process. Thus, the SG provides an effective treatment of corners with conforming elements, which includes the type of corners produced by interface configurations.

Remark 3 Free interface

Another special situation worth mentioning is illustrated in Figure 5. This configuration arises in applications such as the transmission problem in wave scattering [21], and in this terminology the scattering object is completely embedded in the host material. In this case the interface forms the entire boundary surface for the inclusion sub-region. The SG algorithm in this case is straightforward, the boundary integral equations for the object consisting solely of interface equations. The coefficient matrix will take the form of Eq. (13), with the first row and column removed, and hence, is clearly symmetric.

Remark 4 Computational Savings

As in the SG formulation for a non-interface problem, the primary computational advantage of the symmetric formulation is in the reduced time required to solve the system of equations. For a direct solution, this is on the order of $N^3/6$ versus $N^3/3$ for a non-symmetric matrix. Thus, for sufficiently large problems, this factor of two can translate into significantly less computational time [14]. Some savings can be realized in constructing the matrix, but in general this is unfortunately limited: although the coefficient matrix is symmetric, the contributions to the right hand side vector must still be computed for each equation. Thus, the number of calculations that can be bypassed due to symmetry is, speaking somewhat loosely (as this can depend upon the equation being solved), not large relative to the total operations required.

For interface problems, however, the symmetry of the coefficient matrix can be used to good advantage. Note that in (13) the upper right 2×2 block need not be calculated, due to symmetry. These matrix elements come from the boundary integral equations written

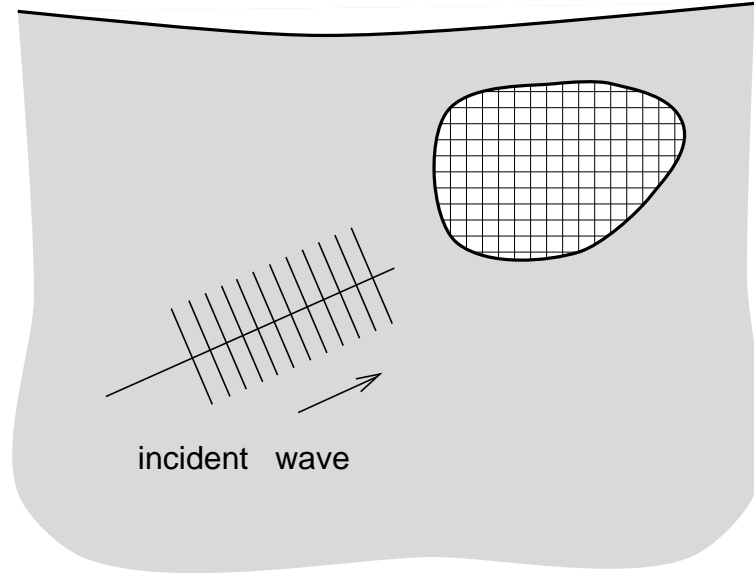


Figure 5: The interface boundary can comprise the entire boundary of a subdomain, as in this wave scattering/transmission problem.

for the non-interface boundaries, integrating over the interface. As indicated above, the only reason for now integrating over the interface in these equations is for constructing the right hand side vector. However, as there are no boundary conditions on the interface, there is *no contribution* to the right hand side. Thus, in forming the equations for the non-interface boundary, *integration over the interface is not required*. Depending upon the geometry of the problem, this can result in considerable computational savings. For instance, for the prototype problem considered in the next section, invoking this symmetry, *i.e.* bypassing the interface integrations for the non-interface equations, produced roughly a 13% reduction in total computation time – 1.05 seconds versus 1.21 seconds. For this relatively small problem (102 nodes), the matrix solution time is minimal, and thus the percent reduction (measured with total time) will be less when larger matrices are involved. Nevertheless, it is clear that a significant amount of computation has been avoided. The 13% number is consistent with related Symmetric Galerkin fracture calculations. In this case, integrations over the crack surface can be skipped when forming the non-crack equations [17].

Remark 5 Related Work

At the final stage of this work, we became aware of related work by Layton et al. [23]. They have used the symmetric Galerkin concept to develop a multi-zone BEM formulation

which results in a partially symmetric coefficient matrix. The symmetry is restricted to the non-interface degrees of freedom of each zone, and the degrees of freedom associated with the interfaces lead to non-symmetric sub-blocks. They demonstrate that condensing out the symmetric portion of the system and solving the resulting reduced non-symmetric system leads to an effective algorithm. However, these authors note that a fully symmetric formulation, as presented herein, would be highly advantageous. For large scale calculations, the condensation techniques discussed in [23] would still prove useful when applied to the present fully symmetric system. In this case, the condensation process is similar to the substructuring techniques in the FEM [24].

5 Calculations

A prototype numerical example modeling heat transfer in an eccentric annulus geometry is considered. To validate the interface algorithm, several variations in the boundary conditions and material properties are examined. This problem has characteristics which make it very suitable for a testing purposes, *e.g.* curved boundaries, a non-convex region, and an interesting (*i.e.* non-trivial) corner situation at the interface junctions. The basic interpolation approximation employed in these tests consists of standard isoparametric, conforming, linear elements.

Figure 6 shows the geometry, boundary conditions, and material properties for the first calculation. The thermal conductivities for the top and bottom parts are denoted by k_A and k_B , respectively. If only one material is present, *i.e.* $k_A = k_B$, then there is a closed form solution for this problem. This solution can be obtained by means of conformal mapping and complex variable techniques, and it is given by (see, for example, the book by Greenberg [25]):

$$\phi = 100 \left[1 - \frac{\ln(u^2 + v^2)}{2 \ln a} \right] , \quad a = 2 + \sqrt{3} , \quad (16)$$

where

$$u(x, y) = \frac{(ax - 1)(x - a) + ay^2}{(ax - 1)^2 + a^2 y^2} , \quad v(x, y) = \frac{(a^2 - 1)y}{(ax - 1)^2 + a^2 y^2} . \quad (17)$$

To verify the computer code, the material constants k_A and k_B were set equal ($k_A = k_B = 1.0$), and the problem solved using interfaces as shown in Figure 6.¹ The boundary element mesh employed for the top half of the domain is shown in Figure 7, the

¹Note that for the single material case, one could take advantage of symmetry and model only the top (or bottom) part of the problem. However, the goal here is to test the interface algorithm.

discretization for the bottom half is identical. A comparison of the theoretical solution (Eqs. (16) and 17)) with the numerical solution is provided in Tables 2, 3, 4, and 5 for some representative points along the boundary. The actual matching interface fluxes are zero, and the SG-BEM values were of the order of 10^{-12} or less. These results indicate that the SG interface algorithm is correct.

Table 2: Flux at the top semi-circle with radius = 1.0.

Angle (rad)	$\partial\phi/\partial\mathbf{n}$		
	Theory	SG-BEM	Error(%)
0	131.5187	133.7729	-1.71
$\pi/4$	101.7244	101.2764	0.44
$\pi/2$	65.7595	65.4230	0.51
$3\pi/4$	48.5829	48.4524	0.27
π	43.8397	44.7766	-2.14

Table 3: Flux at the top semi-circle with radius = 0.25

Angle (rad)	$\partial\phi/\partial\mathbf{n}$		
	Theory	SG-BEM	Error(%)
0	-350.7162	-346.1688	1.30
$\pi/4$	-334.3935	-329.7187	1.40
$\pi/2$	-300.6147	-300.2498	0.12
$3\pi/4$	-273.0345	-269.2404	1.40
π	-263.0383	-259.4839	1.35

The more interesting situation, $k_A \neq k_B$, has also been investigated. For example, if $k_A = 1/2$ and $k_B = 1.0$, then the numerical solution on the bottom semicircles is essentially the same as before, but now the fluxes on the top semicircles are half of what they were before. This happens because the actual matching flux across the interface is zero. The boundary element solution in this case was consistent with this observation, and thus provides additional validation of the present numerical solution procedure for interface problems.

A new boundary value problem for the eccentric annulus configuration is shown in Figure 8. Since there is no analytical solution available for this problem, the SG-BEM results will be compared with those obtained by a FEM calculation. The finite element mesh for the problem of Figure 8 is shown in Figure 9. The graphs in Figures 10 to 15 compare the numerical results obtained by the two methods. Figures 10 and 11 compare the nodal

Table 4: Potential at the LHS interface ($y = 0$).

x	ϕ		
	Theory	SG-BEM	Error(%)
-1.0000	100.0000	100.0000	0.00
-0.8333	92.0218	92.2483	-0.25
-0.6667	82.3856	82.6837	-0.37
-0.5000	70.4045	70.8167	-0.59
-0.3333	54.8778	55.5480	-1.22
-0.1667	33.4085	34.0673	-1.97
-0.0833	18.8852	19.4347	-2.91
0.0000	0.0000	0.0000	0.00

Table 5: Potential at the RHS interface ($y = 0$).

x	ϕ		
	Theory	SG-BEM	Error(%)
0.5000	0.0000	0.0000	0.00
0.5625	19.5925	20.1178	-2.68
0.6250	35.7162	36.3434	-1.76
0.7500	61.6269	62.2651	-1.04
0.8750	82.3856	82.8032	-0.51
1.0000	100.0000	100.0000	0.00

temperature on the top semi-circles of radius 1.0 and 0.25, respectively. Note that the results obtained by the two methods are in good agreement.

Figures 12 and 13 compare the nodal flux at the bottom semi-circles of radius 1.0 and 0.25, respectively. In both graphs, the FEM nodal thermal fluxes are average nodal values, except at the endpoints where the corresponding element nodal thermal flux was used. The bullets at the endpoints of these graphs denote the average nodal flux. In Figure 13, there is a relatively small gap between the SG-BEM and the FEM curves. This is probably due to the coarse boundary element discretization of the bottom semi-circle of radius 0.25 (see Figure 7).

Figure 14 shows a comparison of the computed nodal temperature along the interface, the two curves stemming from the left and right segments of the interface. It is interesting to observe that the results obtained by the two methods are within plotting accuracy. Figure 15 is the corresponding comparison for the interface flux, and three types of results obtained with the FEM are displayed in this figure. 'FEM(average)' means nodal averaging, which should not be used since there are different materials at each side of the interface. 'FEM(average top)' refers to the average nodal flux considering the elements above the interface. These results compare quite well with the SG-BEM. 'FEM(average bottom)' denotes the average nodal flux considering the elements below the interface. This graph illustrates the danger of using average derivative values when different materials are present. In this case, care should be taken to consider appropriate averaging of nodal quantities.

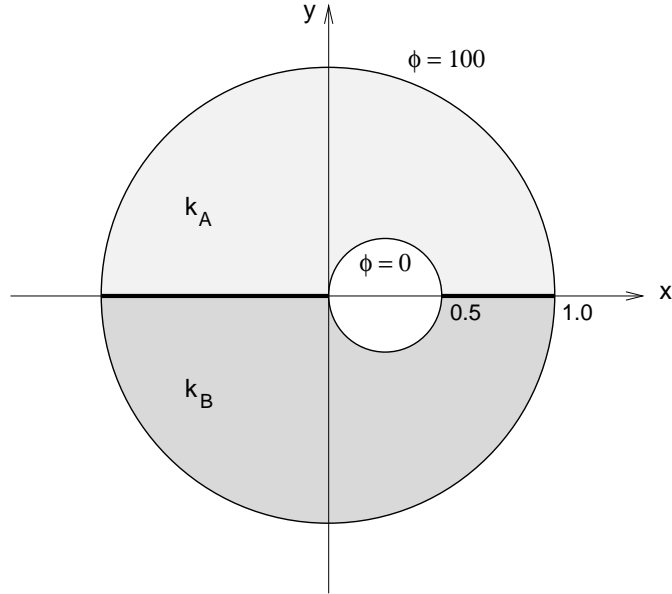


Figure 6: Geometry, boundary conditions and material properties for heat conduction in an eccentric annulus with two types of material.

6 Conclusions and Extensions

This paper has demonstrated that a fully symmetric Galerkin boundary integral equation formulation can be achieved for interface and multi-zone problems. The standard (*i.e.* single domain) SG formulation is based on use of the *dual equations* (*i.e.* the BIE and the HBIE) according to the type of *boundary conditions*. The double integration over the boundary, together with the symmetry properties of the kernels guarantees that the system matrices are symmetric. This approach on the non-interface boundaries, together with a strategic use of both equations on the interface, yields a symmetric system, while automatically incorporating the *continuity conditions* on the interface. The present interface formulation is therefore a natural extension of the SG procedure.

The two most important benefits provided by this boundary integral approach to interface problems are (a) a symmetric coupling of boundary and finite elements, and (b) a computationally efficient algorithm. In a single domain SG algorithm, the efficiency arises from the linear algebra phase of the calculation, solving a symmetric versus a non-symmetric system. However, for an interface problem, the symmetry can be profitably invoked in the matrix construction phase. In constructing the outer boundary equations, integrations over the interface can be bypassed, clearly a considerable bonus for this approach. De-

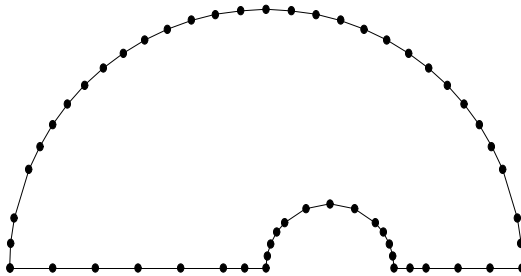


Figure 7: Boundary element mesh (58 nodes and 54 elements) considering the symmetric part of the eccentric annulus. The corresponding mesh for the interface calculations, obtained by symmetry with respect to the horizontal line ($y = 0$), has 116 nodes and 108 elements.

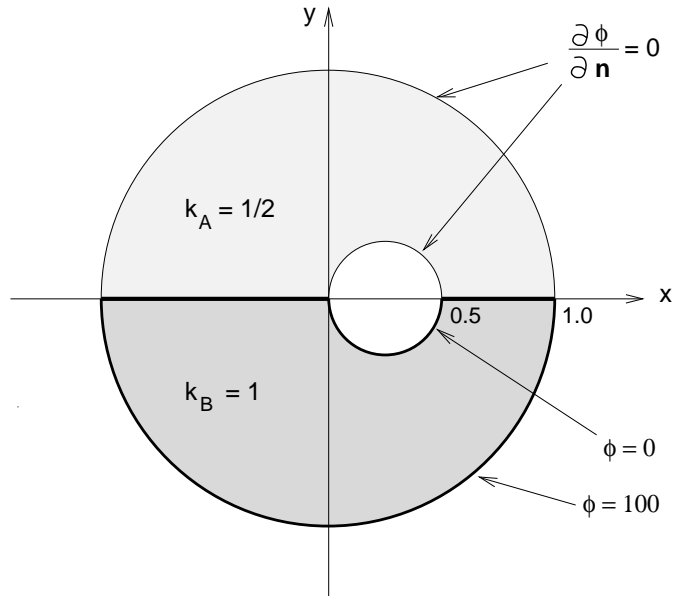


Figure 8: Geometry, new boundary conditions and material properties for heat conduction in an eccentric annulus.

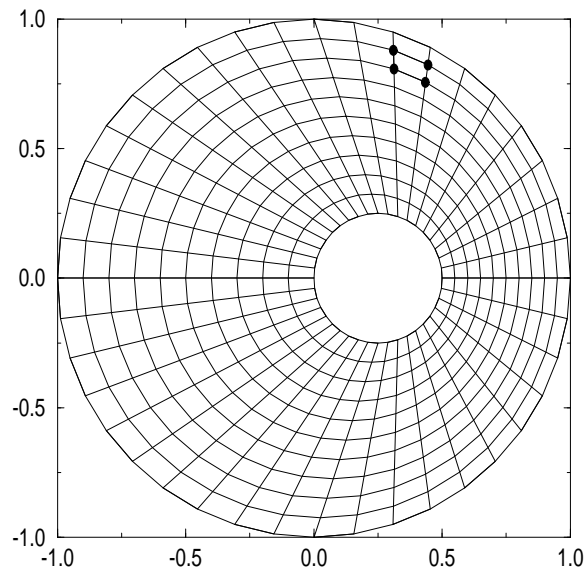


Figure 9: Finite element mesh (440 nodes and 400 elements) for the problem of Figure 8.

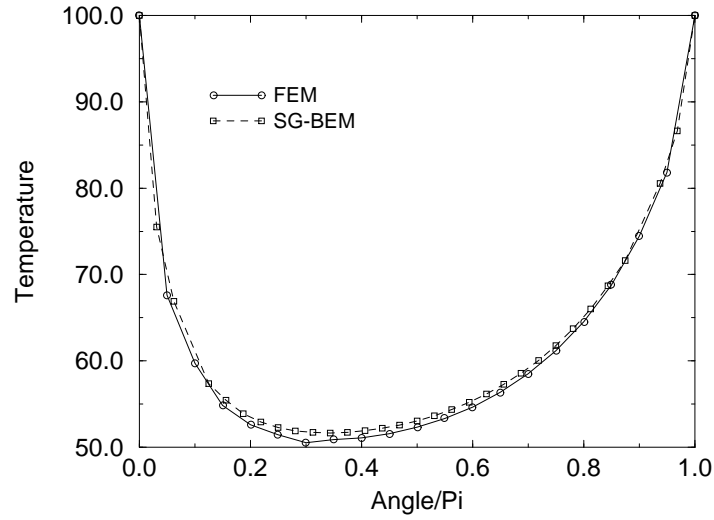


Figure 10: Comparison of the nodal temperatures at the top semi-circle of radius = 1.0 obtained by the FEM and the SG-BEM.

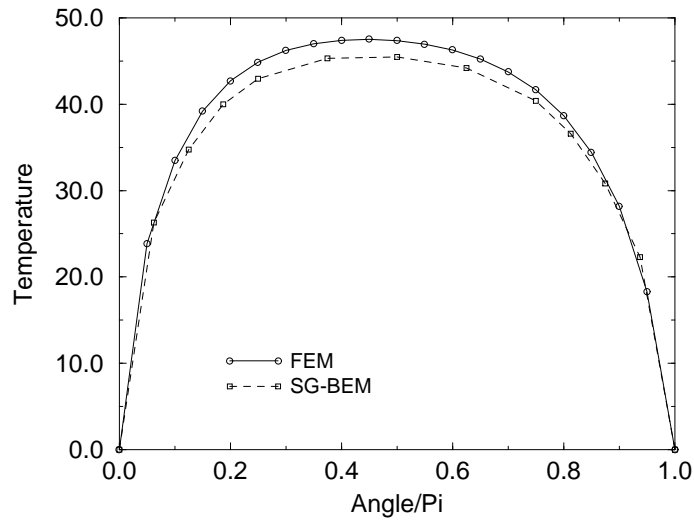


Figure 11: Comparison of the nodal temperatures at the top semi-circle of radius = 0.25 obtained by the FEM and the SG-BEM.

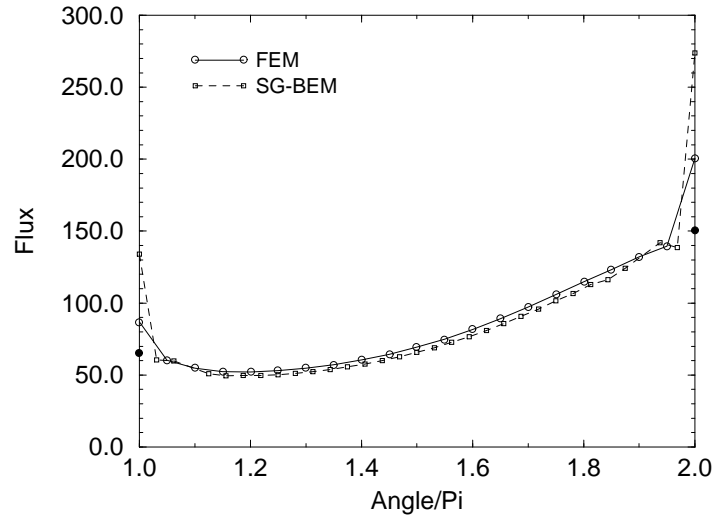


Figure 12: Comparison of the nodal flux at the bottom semi-circle of radius = 1.0 obtained by the FEM and the SG-BEM. The bullets at the endpoints of the graph denote the average FEM nodal flux.

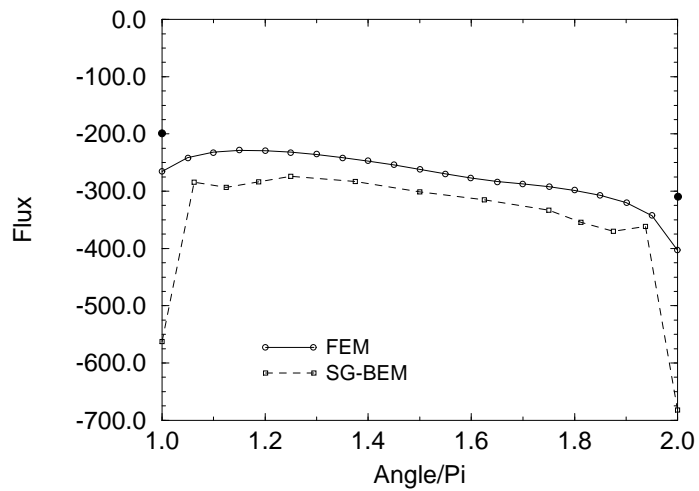


Figure 13: Comparison of the nodal flux at the bottom semi-circle of radius = 0.25 obtained by the FEM and the SG-BEM. The bullets at the endpoints of the graph denote the average FEM nodal flux.

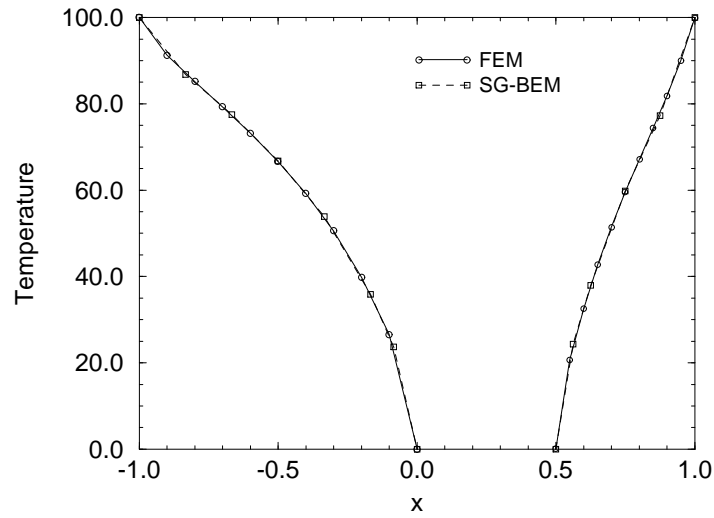


Figure 14: Comparison of the nodal temperatures *along the LHS and RHS interfaces* obtained by the FEM and the SG-BEM.

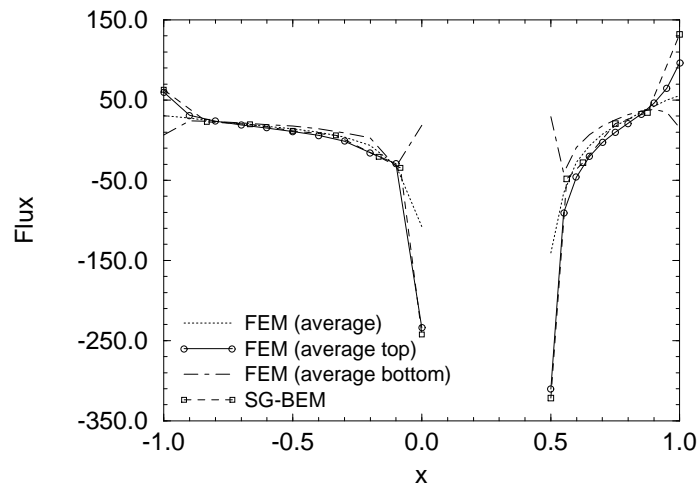


Figure 15: Comparison of the nodal flux *along the LHS and RHS interfaces* obtained by the FEM and the SG-BEM.

tailed timing comparisons with equivalent FEM calculations have not been performed in the work, but should be carried out.

Numerical examples involving heat transfer in an eccentric annulus geometry, with several variations in the boundary conditions and material properties, were considered. These results were in good agreement with analytical solutions, when available, and with numerical solutions obtained with finite elements.

Although a two dimensional scalar field formulation was discussed herein, there is no difficulty in extending this method to three dimensional and vector-field problems. Fracture problems were also not considered, but this algorithm clearly provides an effective framework for studying interfacial cracks. Coupling this approach with special elements for capturing crack tip singularities, or interface corner singularities (as occur in multi-material thermoelastic problems), should be possible, but requires further investigation. The interface formulation should also be directly applicable to nonlinear analysis, in particular the Symmetric Galerkin formulation for plasticity developed by Maier and co-workers [26, 4, 27]. Finally, it is expected that this technique can be naturally incorporated into a general SG error estimation and adaptivity procedure [28]. Investigations in these areas are currently being pursued.

Acknowledgement

This research was partially supported by the Applied Mathematical Sciences Research Program of the Office of Mathematical, Information, and Computational Sciences, U.S. Department of Energy under contract DE-AC05-96OR22464 with Lockheed Martin Energy Research Corp. LJG would like to thank Prof. M. R. Ramey for hospitality at UC-Davis while this work was performed. GHP acknowledges the "Junior Faculty Research Fellowship" from the UC-Davis Academic Senate.

References

- [1] J. N. Reddy and A. Miravete. *Practical Analysis of Composite Laminates*. CRC Press, Boca Raton, 1995.
- [2] James H. Kane. *Boundary Element Analysis in Engineering Continuum Mechanics*. Prentice Hall, New Jersey, 1994.
- [3] F. Hartmann, C. Katz, and B. Protopsaltis. Boundary elements and symmetry. *Ingenieur-Archiv*, 55:440–449, 1985.
- [4] G. Maier, G. Novati, and S. Sirtori. On symmetrization in boundary element elastic and elastoplastic analysis. In G. Kuhn and H. Mang, editors, *Discretization methods in structural mechanics*, pages 191–200. Springer-Verlag, Berlin and New York, 1990.
- [5] C. A. Brebbia, J. C. F. Telles, and L. C. Wrobel. *Boundary element techniques*. Springer-Verlag, Berlin and New York, 1984.
- [6] G. Krishnasamy, F. J. Rizzo, and T. J. Rudolphi. Hypersingular boundary integral equations: Their occurrence, interpretation, regularization and computation. In P. K. Banerjee and S. Kobayashi, editors, *Developments in Boundary Element Methods - Advanced Dynamic Analysis*, volume 7, chapter 7. Elsevier Applied Science Publishers, 1991.
- [7] P. A. Martin and F. J. Rizzo. Hypersingular integrals: how smooth must the density be? *Int. J. Numer. Meth. Engrg.*, 39:687–704, 1996.
- [8] T. J. Rudolphi. Higher order elements and element enhancement by combined regular and hypersingular boundary integral equations. In B. S. Annigeri and K. Tseng, editors, *Boundary Element Methods in Engineering*, pages 448–455, Berlin and New York, 1990. Springer-Verlag.
- [9] K. Tomlinson, C. Bradley, and A. Pullan. On the choice of a derivative boundary element formulation using Hermite interpolation. *International Journal for Numerical Methods in Engineering*, 39(3):451–468, 1996.
- [10] H. G. Walters, J. C. Ortiz, G. S. Gipson, and J. A. Brewer. Overhauser boundary elements in potential theory and linear elastostatics. In T. A. Cruse, editor, *Advanced Boundary Element Methods*, volume 16, pages 459–464, Berlin and New York, 1988. Springer-Verlag.

- [11] W. S. Hall and T. T. Hibbs. The treatment of singularities and the application of the C^1 Overhauser continuous quadrilateral boundary element to three dimensional elastostatics. In T. A. Cruse, editor, *Advanced Boundary Element Methods*, volume 16, pages 135–144, Berlin and New York, 1988. Springer-Verlag.
- [12] L. J. Gray, Luiz F. Martha, and A. R. Ingraffea. Hypersingular integrals in boundary element fracture analysis. *Int. J. Numer. Meth. Engrg.*, 29:1135–1158, 1990.
- [13] G. Krishnasamy, L. W. Schmerr, T. J. Rudolphi, and F. J. Rizzo. Hypersingular boundary integral equations: Some applications in acoustic and elastic wave scattering. *J. Appl. Mech.*, 57:404–414, 1990.
- [14] C. Balakrishna, L. J. Gray, and J. H. Kane. Efficient analytical integration of symmetric Galerkin boundary integrals over curved elements; thermal conduction formulation. *Comput. Methods Appl. Mech. Engrg.*, 111:335–355, 1994.
- [15] C. Balakrishna, L. J. Gray, and J. H. Kane. Efficient analytical integration of symmetric Galerkin boundary integrals over curved elements; elasticity formulation. *Comput. Methods Appl. Mech. Engrg.*, 117:157–179, 1994.
- [16] L. J. Gray, C. Balakrishna, and J. H. Kane. Symmetric Galerkin boundary integral fracture analysis. *Engrg. Analy. Boundary Elements*, 15:103–109, 1995.
- [17] L. J. Gray and G. H. Paulino. Symmetric Galerkin boundary integral fracture analysis for plane orthotropic elasticity. (submitted).
- [18] S. M. Hölzer. The Symmetric Galerkin BEM in elasticity: FEM/BEM coupling, integration and adaptivity. *Computational Mechanics*. submitted.
- [19] L. J. Gray. Boundary element method for regions with thin internal cavities. *Engrg. Analy. Boundary Elem.*, 6:180–184, 1989.
- [20] E. D. Lutz and L. J. Gray. Exact evaluation of singular boundary integrals without CPV. *Comm. Num. Meth. Engrg.*, 9:909–915, 1993.
- [21] F. J. Rizzo, D. J. Shippy, and M. Rezayat. A boundary integral equation method for radiation and scattering of elastic waves in three dimensions. *Int. J. Numer. Meth. Engrg.*, 21:115–129, 1985.
- [22] L. J. Gray and E. D. Lutz. On the treatment of corners in the boundary element method. *J. Comp. Appl. Math.*, 32:369–386, 1990.

- [23] J. B. Layton, S. Ganguly, C. Balakrishna, and J. H. Kane. A symmetric Galerkin multi-zone boundary element formulation. *Int. J. Numer. Meth. Engrg.* (submitted for publication).
- [24] G. H. Paulino S.-H. Hsieh and J. F. Abel. Recursive spectral algorithms for automatic domain partitioning in parallel finite element analysis. *Comput. Methods in Appl. Mech. Engrg.*, 121(1-4):137–162, 1996.
- [25] M. D. Greenberg. *Foundations of Applied Mathematics*. Prentice-Hall, Englewood Cliffs, New Jersey, 1978.
- [26] G. Maier and C. Polizzotto. A Galerkin approach to boundary element elastoplastic analysis. *Computer Methods in Applied Mechanics and Engineering*, 60:175–194, 1987.
- [27] G. Maier, S. Miccoli, G. Novati, and S. Sirtori. A Galerkin symmetric boundary element method in plasticity: formulation and implementation. In J. H. Kane, G. Maier, N. Tosaka, and S. N. Atluri, editors, *Advances in Boundary Element Techniques*, pages 288–328. Springer-Verlag, Berlin Heidelberg, 1993.
- [28] G. H. Paulino and L. J. Gray. Error estimation and adaptivity for the symmetric Galerkin boundary element method. in preparation.